

Flow in curved channels with a low negative rotation speed

Liqui Wang and K. C. Cheng

Department of Mechanical Engineering, University of Alberta, Edmonton, Alberta, Canada T6G 2G8

(Received 29 August 1994)

Experiments on visualization of stabilizing and destabilizing flow in channels with curvature and rotation are described. Two test sections have been used, i.e., the rectangular channels with aspect ratios of 1 and 10, respectively. The results show the end view of flows in the region with a low negative rotation speed. In addition, a generalized Rayleigh criterion is formulated about the primary instability of flows in rotating curved channels to help in understanding the experimental results.

PACS number(s): 47.60.+i, 47.20.Cq, 47.20.Gv, 47.32.-y

I. INTRODUCTION

The curvature and rotation of a channel can stabilize the channel flow in some flow domains and destabilize the flow in other domains. This was first recognized by Reynolds in 1884 [1]. The knowledge of this stabilizing or destabilizing phenomenon is essential in order to have the ability to predict and control the performance for technical applications of the flow in blade passages of radial flow pump, compressor impellers, centrifuges [2], cooling channels of rotating machinery [3–6], particle separation devices [7–11], and rotating heat exchangers [12,13].

The mechanism for this stabilizing or destabilizing phenomenon can be intuitively understood. For flows over convex surfaces, the centrifugal force is mainly balanced by a normal pressure gradient. The fluid particles moving outward across streamlines into regions of higher velocity should on average retain some memory of their previous (lower) velocity history. Their individual centrifugal forces will thus be less than the new normal pressure gradient, resulting in a net restoring force. Therefore, convex boundary layers should act as a stabilizing influence on the flow. On concave surfaces, the opposite destabilizing effect should occur.

The spanwise rotation of a straight channel introduces Coriolis forces into the flow which play a role similar to that of the centrifugal forces in curved channels. Here the flows near the antirotating wall are destabilized, while the flows near the corotating wall are stabilized. By the *antirotating (corotating) wall* we mean the side on which the imposed rotation and the basic flow vorticity have the opposite (same) sense. They are also called pressure (leading) and suction (trailing) walls, respectively.

The combined effects of both curvature and rotation occur in a curved channel with spanwise system rotation. Depending on the direction of rotation, the stabilizing or destabilizing effects due to the curvature and the rotation will either enhance or counteract each other. The stabilizing and destabilizing flows in a curved rotating channel are then endowed with some more complex features.

Early works have been constrained to the two simplified limiting cases, i.e., weak rotations or strong rotations. By employing Pohlhausen's method, Ludweig [14] and Hocking [15] examined the fully developed lamina-

nar boundary layers in a rotating curved channel with a square and a rectangular cross section, respectively. Their results are valid for a large rotational Reynolds number based on the angular velocity of the channel, as compared to the usual Reynolds number based on the mean axial velocity of the fluid. This problem is not considered to be as difficult as the case with moderate rotation since the flow in the interior of the channel is approximately geostrophic. By finite-difference method, Miyazaki [4,5] numerically analyzed the fully developed laminar flow and heat transfer in curved, rotating, circular and rectangular channels. Because of the convergence difficulties of the iterative solution method used, Miyazaki's works were limited to the case of weak rotations. In addition, all the works employ a steady model for the fully developed laminar flows with a positive rotation of the channel. Hereinafter, *positive rotation* means that the rotation is in the same direction as the axial flow imposed by a pressure gradient and *negative rotation* means that the rotation opposes the flow due to the pressure gradient.

Because of these limitations, the secondary flow revealed by the works mentioned above consists of one pair of counterrotating vortices in a plane perpendicular to the axis of the channel. The interaction of the secondary flow with the pressure-driven main flow shifts the location of the maximum axial velocity away from the center of the channel and in the direction of the secondary velocity in the middle of the channel.

More comprehensive analytical and numerical studies have been made recently in [16–19] for the circular tubes and in [20–22] for the square channels. All the works also assume the flow to be steady, laminar, and fully developed, but cover a rather wide range of parameters. In particular, the works contain the effect of the rotation directions and the rotation speed ranges from a weak rotation to a strong rotation. When the rotation is positive, the flow structure is found to be similar to that observed in stationary channels [23–32] or spanwisely rotating straight channels [6,33–36], i.e., with one or two pairs of secondary flow vortices in addition to the axial flow. When the rotation is negative, the inward Coriolis forces can completely destroy the Dean vortices and give rise to the Coriolis vortices on the convex (inner) wall. Furthermore, they may cause the direction of the secondary flow

to reverse by overcoming the outward centrifugal forces.

A striking feature of the flow reversal is that it occurs after passing through a region of flow of multiple pairs of vortices where the channel rotates at a slow negative rotation speed. In this region, the values of the rotation number Ro [the inverse of a Rossby number, Eq. (10)] have the order of the curvature ratio σ of the channel [Eq. (10)]. Note that the mechanism of the appearance of the flow of multiple pairs of vortices has been left unsolved. In addition, it appears that no experimental work has been reported to show the flow in this region.

In the present work, a smoke visualization apparatus is designed to visualize the flow in the curved channels rotating spanwisely with a low negative rotation speed. Two channels are used. In addition, a generalized Rayleigh stability criterion, including effects of both centrifugal and Coriolis forces, is formulated for the flows in the channels with an infinite span. The objectives of this study are to give some qualitative information about the flows as observed from flow visualizations and photographs and to explore the mechanism of the appearance of the flow of multiple pairs of vortices.

II. EXPERIMENTAL APPARATUS AND TECHNIQUE

A schematic diagram of the experimental apparatus is shown in Fig. 1. It consists of a test section, a rotating table with a rotating seal, an air supply system, and a smoke generator.

The rotating table is driven by an electric motor with adjustable speed drive and the range of the rotating speed is $n=0\sim 500$ rpm. The rotational speed is measured by using an optical slot switch running on a disk with 60 equally spaced holes near its perimeter. The signal from the switch is fed to a Hewlett Packard HP 5314A Universal counter. With 60 holes in the disk, the frequency in hertz equals the rotational speed in rpm.

A second disk with a single hole provides the signal for firing the General Radio 1540 Strobolume by way of a delay generator and single flash flip-flop which allows visual observation using a slit light source with one flash per rotation and also permits a single, properly timed flash for photographing the whole flow field.

The building compressed air is used as the fluid. The

air flow rate is measured by a Meriam flow element with a calibrated differential pressure transducer. The smoke generated by burning Chinese incense sticks is injected through a dispersing tube before the test section as shown in Fig. 1. The very tiny smoke particle, subjected to neglected gravitational and rotational buoyancy forces relative to the drag forces, marks fluid particle trajectories. The smoke patterns are photographed instantly at the exit of the test section, revealing the flow pattern. This provides an end view of the secondary flow pattern for an observer looking upstream into the channel cross section. A Nikon FM2 single lens reflex camera and Kodak T-Max black and white film P3200 are used.

Two test sections (TSs), denoted by TS *A* and TS *B*, are shown in Fig. 2. TS *A* consists of an entrance spiral square channel with an axial length of 0.85 m and a curved square channel (270° bend with an axial length of 1.2 m) with a constant radius of curvature $R_c=25.4$ cm. The top view and the exit cross section are shown in Fig. 2(a). The curved square channel has a cross section of 5.08×5.08 cm². The air flows through a rotating straight tube (with an inside diameter of 4 cm) along the axis of rotation and then enters the spiral square channel before entering the test section. The test section was made from acrylic sheets.

TS *B*, also made from acrylic sheets, consists of an entrance spiral rectangular channel with an axial length of 1.25 m and a curved rectangular channel (270° bend) with a constant radius of curvature $R_c=25.4$ cm. The top view and the exit cross section for TS *B* are shown in Fig. 2(b). The air flows through a rotating straight tube (with an inside diameter of 4 cm) along the axis of rotation and then enters the spiral rectangular channel before flowing into the curved channel.

III. RESULTS AND DISCUSSION

The end-view photographs are to be shown for TS *A* and TS *B* with the spanwise direction vertical and the radial direction horizontal. In each photograph, the convex (inner) wall is on the left and the concave (outer) wall is on the right. A different test condition for a given test section is characterized by two parameters, namely, the Reynolds number Re and the rotation number Ro . The channel width a is used as the characteristic length in Re

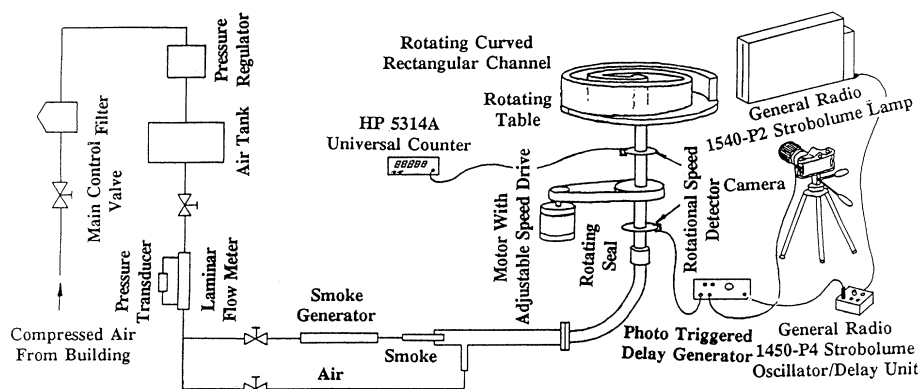


FIG. 1. Schematic diagram of the experimental apparatus.

and Ro ($Re = W_m a / \nu$ and $Ro = \Omega a / W_m$, where W_m is the mean axial velocity, ν is the kinematic viscosity of air, and Ω is the angular rotation speed of the channel). For a given set of Re and Ro , several photographs, each taken at a different instant, are usually given to show the time variation of the flow.

Examples of smoke patterns from the multipair vortex flow are illustrated in Fig. 3 for TS *A* and in Fig. 4 for TS *B*. They are obtained at $Re = 500$, $Ro = -0.330$; $Re = 600$, $Ro = -0.274$; $Re = 1000$, $Ro = -0.279$; and $Re = 2000$, $Ro = -0.165$ for TS *A* and at $Re = 110$, $Ro = -0.0792$ and $Re = 452$, $Ro = -0.0914$ for TS *B*. The patterns are especially interesting because they show the existence of the flow of multiple pairs of vortices.

In order to understand the mechanism, we use a displaced particle argument [37] to derive a stability criterion including both centrifugal and Coriolis force effects. This can be regarded as the generalization of

Rayleigh's theory to include both curvature and rotation effects.

To simplify the analysis, consider an undisturbed flow in a rotating curved channel with an infinite span, as shown in Fig. 5. If a fluid particle moving with streamwise velocity w at a distance r from the center of curvature o is displaced by a radial disturbing force, the variation in the moment of the momentum of the particle, taken around the axis perpendicular to w through o , can be written as (applying the principle of moment of momentum)

$$\bar{W}(r + dr) - Wr = -2\Omega \int_0^{\Delta t} vr dt, \quad (1)$$

where v is the displacement speed and Δt the time required for the particle to move from r to $r + dr$. This gives the streamwise velocity \bar{W} of the particle at the new position

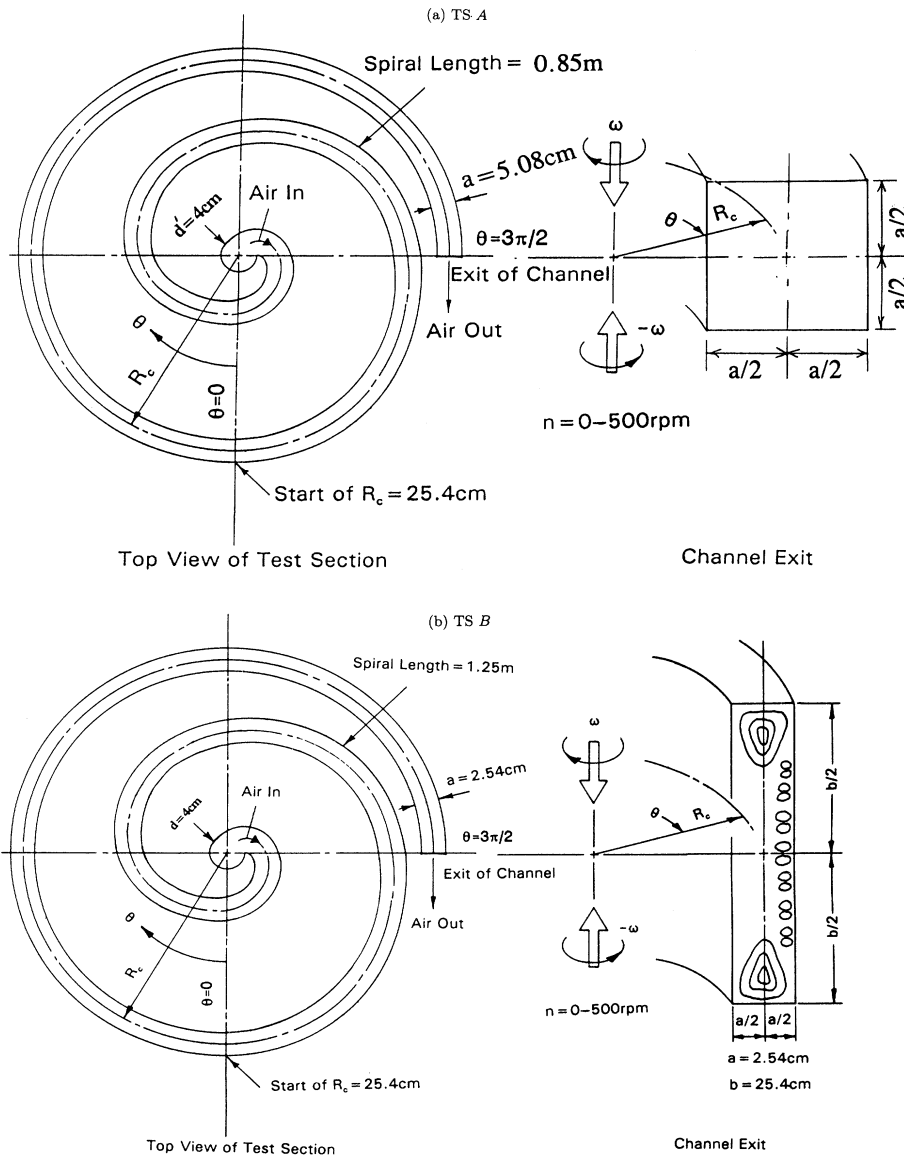


FIG. 2. Two test sections.



(a) $Re = 500, Ro = -0.330$



(b) $Re = 600, Ro = -0.274$



(c) $Re = 1000, Ro = -0.279$



(d) $Re = 2000, Ro = -0.165$

FIG. 3. Flows in the region with two unstable layers for TS A.

$Re = 110, Ro = -0.0792$



$Re = 452, Ro = -0.0914$



FIG. 4. Flows in the region with two unstable layers for TS B.

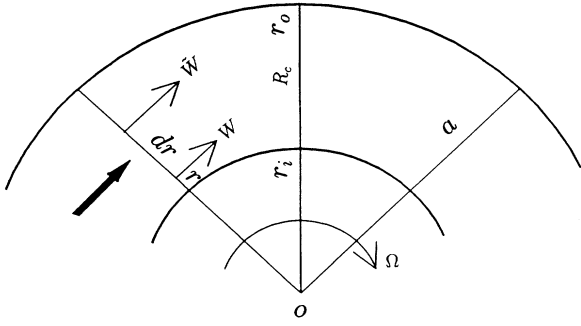


FIG. 5. Sketch related to the discussion of the displaced particle.

$$\tilde{W} = W - \frac{Wdr}{r} - 2\Omega dr \quad (2)$$

to the first order of dr .

With a streamwise velocity \tilde{W} , the particle at the new position is subjected to a centrifugal force F_1 and a Coriolis force F_2 along the radial direction as

$$F_1 = \frac{\rho \tilde{W}^2}{r + dr}, \quad F_2 = 2\rho\Omega \tilde{W}. \quad (3)$$

In the undisturbed flow, the centrifugal force and Coriolis force acting on a particle with a streamwise velocity $W + (dW/dr)dr$ at $r + dr$ is balanced by a pressure gradient in the radial direction, i.e.,

$$\frac{\partial P}{\partial r} \Big|_{r+dr} = \rho \frac{\left[W + \frac{dW}{dr} dr \right]^2}{r + dr} + 2\rho\Omega \left[W + \frac{dW}{dr} dr \right]. \quad (4)$$

This pressure gradient will also act on the displaced particle [37]. Hence the restoring force per unit volume acting on the displaced particle is [Eqs. (3) and (4)]

$$F = \rho \frac{\left[W + \frac{dW}{dr} dr \right]^2}{r + dr} + 2\rho\Omega \left[W + \frac{dW}{dr} dr \right] - \frac{\rho \tilde{W}^2}{r + dr} - 2\rho\Omega \tilde{W}. \quad (5)$$

Substituting Eq. (2) into Eq. (5) gives

$$F = \rho\Theta(r)dr + o(dr^2), \quad (6)$$

where

$$\Theta(r) = \frac{2W}{r} \left[\frac{dW}{dr} + \frac{W}{r} \right] + \frac{6\Omega W}{r} + 2\Omega \left[\frac{dW}{dr} + 2\Omega \right]. \quad (7)$$

Nondimensionalizing $\Theta(r)$, Ω , W , and r by $(W_m/a)^2$, W_m/a , W_m , and a , with W_m as the mean streamwise velocity across the channel [$W_m = (1/a) \int_{r_i}^{r_o} W(r) dr$], we have

$$\Pi = \frac{\Theta}{(W_m/a)^2} = 2 \left[\frac{\sigma w}{1 + \sigma(x - \frac{1}{2})} + \text{Ro} \right] \times \left[\frac{dw}{dx} + \frac{\sigma W}{1 + \sigma(x - \frac{1}{2})} + 2\text{Ro} \right] \quad (8)$$

or

$$\Pi = \frac{2\sigma w}{1 + \sigma(x - \frac{1}{2})} \left[\frac{dw}{dx} + \frac{\sigma w}{1 + \sigma(x - \frac{1}{2})} \right] + \frac{6\sigma w \text{Ro}}{1 + \sigma(x - \frac{1}{2})} + 2\text{Ro} \left[\frac{dw}{dx} + 2\text{Ro} \right], \quad (9)$$

where

$$x = \frac{r-R}{a}, \quad w = \frac{W}{W_m}, \quad \text{Ro} = \frac{\Omega a}{W_m}, \quad \sigma = \frac{a}{R_c}. \quad (10)$$

Ro , the inverse of a Rossby number, represents the ratio of the Coriolis force to the inertia force.

Π may be called the generalized Rayleigh stability criterion, which includes effects of both centrifugal and Coriolis forces. The second term on the right-hand side of Eq. (9) is the coupling term between the curvature and rotation, while the first and third terms are the centrifugal instability-related and the Coriolis instability-related effects, respectively. The flow is stable in the flow domain with $\Pi > 0$ and unstable in the domain with $\Pi < 0$.

For the flow in a curved channel with rotation around the axis of curvature, the base flow is unaffected by the rotation [38]. Chandrasekhar [38] obtained a solution for the base flow. For the small gap ($\sigma \ll 1$), it can be written as

$$w(x) = 6x(1-x). \quad (11)$$

Next we analyze the stable and unstable regions through Eq. (8) or (9) for one special case, namely, a small gap with a low rotation rate.

For the small gap ($\sigma \ll 1$) and low rotation rate

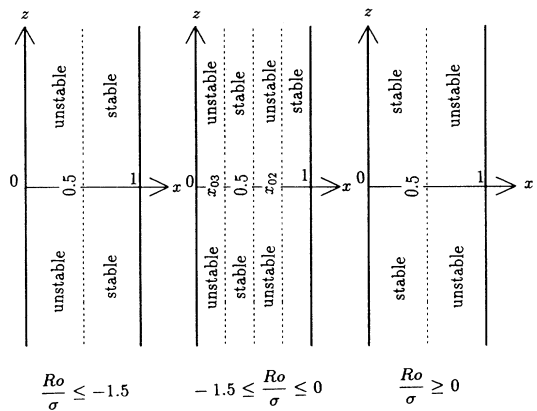


FIG. 6. Stable and unstable regions for the case of a small gap with low rotation rate.

TABLE I. Sign of Π for the case of small gap and low rotation rate.

Ro/σ	Region with positive Π	Region with negative Π
$Ro/\sigma \leq -1.5$	$0 < x < \frac{1}{2}$	$\frac{1}{2} < x < 1$
$-1.5 \leq Ro/\sigma \leq 0$	$x_{03} < x < \frac{1}{2}$ $x_{02} < x < 1$	$0 < x < x_{03}$ $\frac{1}{2} < x < x_{02}$
$Ro/\sigma \geq 0$	$0 < x < \frac{1}{2}$	$\frac{1}{2} < x < 1$

$[Ro \sim o(\sigma)]$, the generalized Rayleigh criterion Π reduces to

$$\Pi = 2(\sigma w + Ro) \frac{dw}{dx} . \quad (12)$$

The condition $\Pi(x)=0$, which can be obtained either by $\sigma w + Ro = 0$ or by $dw/dx = 0$, gives the boundary between the stable region and the unstable region. By $dw/dx = 0$ we have

$$x_{01} = \frac{1}{2} \quad \forall Ro , \quad (13)$$

which is the midplane of the channel. By $\sigma w + Ro = 0$, we have

$$\begin{aligned} x_{02} &= \frac{1}{2} [1 + \sqrt{1 + 2Ro/(3\sigma)}] , \\ x_{03} &= \frac{1}{2} [1 - \sqrt{1 + 2Ro/(3\sigma)}] \end{aligned} \quad (14)$$

for all values of Ro satisfying

$$-1.5 \leq \frac{Ro}{\sigma} \leq 0 . \quad (15)$$

The sign of Π in different regions is listed in Table I. Thus the stable and unstable regions can be determined, as shown in Fig. 6. Although we show all the regions of Ro in Table I and Fig. 6, the results are valid only for lower $|Ro|$ with $Ro \sim o(\sigma)$.

It is interesting that, in the region $-1.5 < Ro/\sigma < 0$, there exist two potentially unstable regions separated by two stable regions. We could expect that the competition of the destabilizing mechanisms in the two regions will

lead to a complicated flow. The flow shown in Figs. 3 and 4 is in or around this region of parameters. Therefore, the appearance of the flow of multiple pairs of vortices comes from the existence of two potential unstable regions alternating by two stable regions in the cross plane.

The oscillating feature of the flow can be inferred by a comparison between the photographs taken at different instants for each case in Figs. 3 and 4. Two resources possibly contribute to this oscillating feature, i.e., the secondary instability of the primary instability or invalidation of the principle of exchange of instabilities in this region. The flow visualization experiments are inappropriate to determine the exact cause. Thus a further detailed stability analysis is required in the future.

IV. CONCLUDING REMARKS

For the flows in a curved channel spanwisely rotating with a low negative rotation speed, there are two potentially unstable regions alternating with two stable layers in the cross plane. The competition of the two destabilizing mechanisms causes the appearance of the flows of multiple pairs of vortices. The flow visualization shows that such flows are associated with the oscillating phenomenon. This suggests further stability analysis for these flows.

-
- [1] O. Reynolds, *Scientific Papers* (Cambridge University Press, Cambridge, 1884), Vol. 2, p. 157.
[2] D. Hochrainer, *J. Colloid Interface Sci.* **36**, 191 (1971).
[3] H. Ito and T. Motai, *Rep. Inst. High Speed Mech.* **29**, 33 (1974).
[4] H. Miyazaki, *Int. J. Heat Mass Transfer* **14**, 1295 (1971).
[5] H. Miyazaki, *J. Heat Transfer* **95**, 64 (1973).
[6] W. D. Morris, *Heat Transfer and Fluid Flow in Rotating Coolant Channels* (Wiley, New York, 1981).
[7] J. W. Lennartz, M. B. Gorenssek, and R. J. Alder, *AIChE J.* **33**, 506 (1987).
[8] J. S. Papanu, R. J. Adler, M. B. Gorenssek, and M. M. Menon, *AIChE J.* **32**, 798 (1986).
[9] M. D. Hoover, W. Stöber, and G. Morawietz, *J. Fluids Eng.* **106**, 38 (1984).
[10] W. Stöber and H. Flachsbart, *Environ. Science Technol.* **3**, 1280 (1969).
[11] P. Kotrappa and M. E. Light, *Rev. Sci. Instrum.* **43**, 1106 (1972).
[12] L. Qiu, L. Wang, and Y. Sun (unpublished).
[13] L. Qiu, L. Wang, and Y. Sun, in *Heat Transfer Enhancement and Energy Conservation*, edited by S. J. Deng, T. N. Veziroğlu, Y. K. Tan, and L. Q. Chen (Hemisphere, New York, 1990).
[14] H. Ludweig, *Ing. Arch.* **19**, 296 (1951).
[15] L. M. Hocking, *J. Math. Phys. Sci.* **1**, 123 (1967).
[16] P. Daskopoulos and A. M. Lenhoff, *J. Fluid Mech.* **217**, 575 (1990).
[17] L. Wang, J. C. Y. Wang, and K. C. Cheng (unpublished).
[18] L. Wang and K. C. Cheng (unpublished).
[19] L. Wang and K. C. Cheng (unpublished).
[20] M. Selmi, K. Nandakumar, and W. H. Finlay, *J. Fluid*

- Mech. **262**, 353 (1994).
- [21] L. Wang and K. C. Cheng (unpublished).
- [22] L. Wang and K. C. Cheng (unpublished).
- [23] K. C. Cheng and M. Akiyama, *Int. J. Heat Mass Transfer* **13**, 471 (1970).
- [24] K. C. Cheng, R. C. Lin and J. W. Ou, *J. Fluids Eng.* **98**, 41 (1976).
- [25] T. J. Pedley, *The Fluid Mechanics of Large Blood Vessels* (Cambridge University Press, Cambridge, 1980), pp. 160–234.
- [26] S. C. R. Dennis and M. Ng, *Q. J. Mech. Appl. Math.* **35**, 305 (1982).
- [27] S. A. Berger, L. Talbot, and L. S. Yao, *Annu. Rev. Fluid Mech.* **15**, 461 (1983).
- [28] K. Nandakumar and J. H. Masliyah, *Adv. Transport Processes* **4**, 49 (1986).
- [29] H. Ito, *JSME Int. J.* **30**, 543 (1987).
- [30] K. H. Winters, *J. Fluid Mech.* **180**, 343 (1987).
- [31] S. A. Berger (unpublished).
- [32] B. Bara, K. Nandakumar, and J. H. Masliyah, *J. Fluid Mech.* **244**, 339 (1992).
- [33] C. G. Speziale, *J. Fluid Mech.* **122**, 251 (1982).
- [34] C. G. Speziale and S. Thangam, *J. Fluid Mech.* **130**, 377 (1983).
- [35] H. S. Khesghi and L. E. Scriven, *Phys. Fluids* **28**, 2968 (1985).
- [36] K. Nandakumar, H. Raszillier, and F. Durst, *Phys. Fluids A* **3**, 770 (1991).
- [37] D. J. Tritton and P. A. Davies, in *Hydrodynamic Instabilities and the Transition to Turbulence*, 2nd ed., edited by H. L. Swinney and J. P. Gollub (Springer, New York, 1985), Vol. 45, pp. 229–270.
- [38] S. Chandrasekhar, *Hydrodynamic and Hydromagnetic Stability* (Oxford University Press, London, 1961).



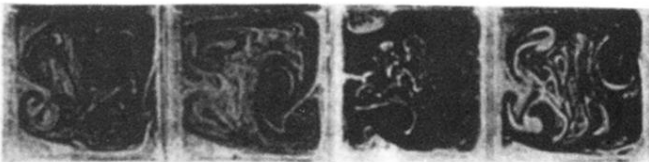
(a) $Re = 500, Ro = -0.330$



(b) $Re = 600, Ro = -0.274$



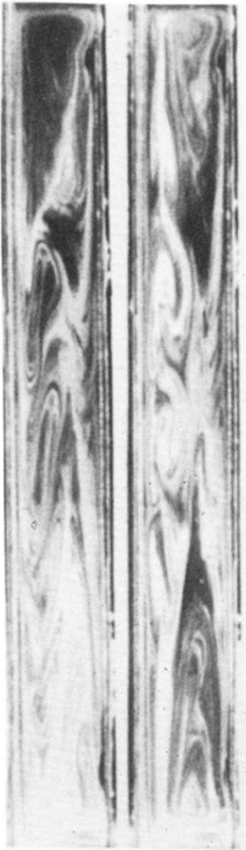
(c) $Re = 1000, Ro = -0.279$



(d) $Re = 2000, Ro = -0.165$

FIG. 3. Flows in the region with two unstable layers for TS A .

$Re = 110, Ro = -0.0792$



$Re = 452, Ro = -0.0914$



FIG. 4. Flows in the region with two unstable layers for TS *B*.